Environmental Science & Technology

pubs.acs.org/est

Article

Mineral Scaling on Reverse Osmosis Membranes: Role of Mass, Orientation, and Crystallinity on Permeability

Meng Wang, Bo Cao, Yandi Hu,*,§ and Debora F. Rodrigues*,§

Cite This: https://doi.org/10.1021/acs.est.1c04143

Read Online

ACCESS | Metrics & More | Article Recommendations | Supporting Information

ABSTRACT: Prior mineral scaling investigations mainly studied the effects of membrane surface properties rather than on the mineral properties and their impact on membrane permeability. In our study, mass, crystal growth orientation, and crystallinity of mineral precipitates on membranes, as well as their effects on membrane permeability have been investigated. Gypsum scaling tests on bare and bovine serum albumin (BSA)-conditioned membranes were conducted under different saturation indices. Results show that a longer scaling period was required for BSA-conditioned membranes to reach the same membrane permeate flux decline as bare membranes. Though the final reduced permeability was the same for both two membranes, the masses of the mineral precipitates on BSA-conditioned membranes were around two times more than those on bare membranes. Further mineral characterizations confirmed that different permeability decay rates of both types of the membrane were attributed to the differences in growth orientations rather than amounts of gypsum precipitates. Moreover, BSA-conditioned layers with high carboxylic density and specific molecular structure could stabilize bassanite and disrupt the oriented growth to inhibit the formation of needle-like gypsum crystals as observed on bare membranes, thus resulting in lower surface coverage with scales on membranes and alleviating the detrimental scaling effect on membrane permeability.

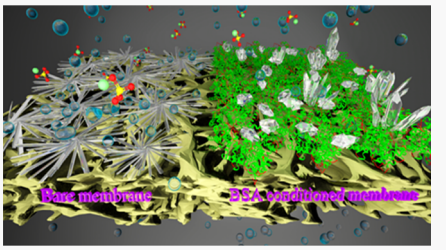

KEYWORDS: *reverse osmosis, calcium sulfate, bovine serum albumin (BSA), bassanite stabilization, crystal growth*

1. INTRODUCTION

Seawater desalination has been considered as a reliable approach to meet the future demand of clean water.[1,2] Reverse osmosis (RO) has gradually become a reliable and advanced desalination method in the past 40 years.[3] However, mineral scaling remains a major problem associated with reverse osmosis operations, which results in higher operation and maintenance costs due to permeability loss, decreased rejection of solute, and irreversible membrane deterioration.[4−6]

Due to the importance of mineral scaling on membranes, recent studies have been conducted to investigate how would different membrane surface properties affect mineral scaling.[7−13] For example, Mi and Elimelech found that different membranes might have distinct gypsum scaling mechanisms due to different interactions between the precipitates and functional groups on the membrane surfaces.[13] Similarly, membrane modification by tuning the surface chemistry has also been demonstrated to affect mineral scaling. For instance, in our recent study, gypsum scaling on GO-modified membranes was shown to be inhibited due to changes on the surface properties of the membrane. In this case, the GO coating enhanced the hydrophilicity and increased the negative charge on the membrane surface, thereby causing less reduction of the membrane permeability.[14,15] Besides, zwitterion polymer brushes were also introduced to modify RO membranes, the delay of gypsum surface nucleation and crystal adsorption were observed on the superhydrophillic surfaces, thus exhibiting a much smaller flux decline than that of control unmodified membranes.[16] Moreover, organic biomolecules (proteins, polysaccharides, and organic acid) are commonly present in natural water and can also attach to the membrane surface, thus altering the membrane surface properties.[7−9,11,12] Liu and Mi revealed that humic acid (HA) and sodium alginate (SA) facilitated gypsum scaling and aggravated the flux decay of the membrane, while bovine serum albumin (BSA) inhibited gypsum scaling and retarded the flux decline. Those organic foulants were also found to affect the morphology of gypsum precipitates, but the role of their amounts and morphologies on flux decline were not elucidated.[12] Similar investigations, with almost identical conclusions, were also conducted by Wang et al.[8] and Bennecke et al.[11] These previous studies have shed some lights on general information gaps related to the impact of membrane surface properties on the types of crystals formed during scaling. However, none of them tried to understand the effect of mass, morphology, growth orientation, and crystallinity of the mineral precipitates on the membrane in the

Received: June 23, 2021
Revised: November 5, 2021
Accepted: November 5, 2021

Table 1. Calcium Sulfate Membrane Scaling Solution Conditions at 25 °C[a]

solution condition	$CaCl_2$ (mM)	Na_2SO_4 (mM)	IS (mM)	pH	Bulk SI_{gyp}	CP	local SI_{gyp}	bulk SI_{bas}
1	20	20	92	5.6	−0.13	1.33	0.02	−0.94
2	30	30	135	5.6	0.07	1.24	0.17	−0.72

[a]Note: (1) CP was determined using the classical film model,[23−25] and the calculation values and details, including the initial membrane permeate flux, CP, and, local SI are presented in the Supporting Information (SI, TexS1, Table S1). (2) SI refers to saturation indices with respect to gypsum and bassanite. $SI = \log_{10}(Q/K_{sp})$, where Q is the actual dissolved composition (i.e. Ca^{2+}, and SO_4^{2-}), and K_{sp} is the solubility constant based on GWB database. The SI results are presented in $\log_{10}$-base.

presence or absence of organic molecules and their roles on the permeability decline of the membrane.

In the present study, we aimed at fulfilling such a significant information gap to bridge the fundamental findings of surface nanochemistry and its roles in mineralization with the engineered application of membrane scaling and permeability control. Calcium sulfate ($CaSO_4$) is usually chosen as the scalant in the above-mentioned studies because of its ubiquitous occurrence, and when crystallized as gypsum, it becomes a difficult scalant to be removed with the usual pH adjustment method.[4] Gypsum crystal formation can typically follow two different scaling pathways: the first one is the classical pathway, which involves the dissolution of bassanite and subsequent recrystallization of gypsum;[17] the second pathway is the non-classical pathway, in which gypsum is formed through the oriented attachment of amorphous precursors (i.e., bassanite), and subsequent crystal growth.[18−21] In the present study, such process was investigated by determining the calcium sulfate scaling on bare and BSA-conditioned membranes. BSA was chosen to condition the membrane because it was previously demonstrated to inhibit gypsum scaling and retard the flux decline.[8,11,12] In this study, three objectives were defined with bare and BSA-conditioned membranes, namely: (1) to establish systematic characterization methods for the amount, crystallinity, and orientation of mineral scales on reverse osmosis membranes; (2) to understand how bare and BSA-conditioned membranes would affect the amount, crystallinity, and orientation of mineral scales; (3) to reveal the relationship between the amount, crystallinity, and orientation of precipitates and the permeability of the membrane. Scaling experiments were conducted using a laboratory RO filtration setup, and the masses, crystallinity, and three-dimensional topology of calcium sulfate precipitates were characterized using atomic absorption spectrometry (AAS), X-ray diffraction (XRD), grazing incidence wide angle X-ray scattering (GIWAXS), and vertical scanning interferometry (VSI). Ex situ atomic force microscopy (AFM) was also used to directly observe the nanoscale morphology of the mineral precipitates.

2. MATERIALS AND METHODS

2.1. Solution Conditions. Calcium sulfate solutions were prepared by sodium sulfate anhydrous (Na_2SO_4) and calcium chloride dehydrate ($CaCl_2{\cdot}2H_2O$) purchased from Fisher-Scientific. The mixed $CaCl_2{\cdot}2H_2O$ and Na_2SO_4 solution compositions, pH, ionic strength, and saturation indices (SI) with respect to gypsum and bassanite were calculated using Geochemist's Workbench (GWB, 11.0. 6, Aqueous Solution LLC, Table 1). Mineral scales formed on the RO membrane surfaces through both heterogeneous crystallization, and deposition of homogeneous precipitates from the bulk solution.[4] Therefore, the experimental conditions were designed to mimic the solution chemistry of brackish water desalination (Table S5, Supporting Information).[22] The first condition (Table 1) was under-saturated with respect to gypsum in bulk solution (Bulk SI_{gyp} = −0.13), while the concentration polarization caused the local solution near the membrane surface to be saturated (Local SI_{gyp} = 0.02). Therefore, only heterogeneous precipitation occurred on the membrane surfaces. The second solution condition (Table 1) was slightly supersaturated with gypsum (Bulk SI_{gyp} = 0.07, Local SI_{gyp} = 0.17), hence, both heterogeneous precipitation and deposition of homogeneous precipitates took place on the membrane. Besides, the bulk solution SI with respect to bassanite (Bulk SI_{bas} = −0.72) was also within the solubility region (SI_{Bas} = −0.02 to −0.72), where nano-bassanite formed first in bulk solution and then transformed into gypsum precipitates.[19] Hence, the second solution condition aimed to help study the possible phase transition during gypsum formation on the membrane surface. In addition, it should be noted that the concentration polarization (CP) on the membrane surface during RO operation causes the local SI at the membrane surface to exceed the bulk SI. Therefore, the local SI was calculated considering the CP effect, as previously described.[14]

2.2. Membrane Conditioning and Scaling Protocols. Membrane conditioning and scaling experiments were conducted using a laboratory-scale RO filtration system.[14] The experimental setup consisted of two tanks: one tank was filled with deionized (DI) water for stabilization and the other tank contained solutions with only BSA or well-mixed salt, which were used for membrane BSA conditioning or scaling, respectively. For each run, the feed solution was continuously recirculated in the RO system with the same cross-flow velocity of 15.8 cm/s and constant transmembrane pressure of 500 psi. In addition, replicate tests for each solution condition were conducted under the same abovementioned conditions to ensure reproducibility and quality control.

Two sets of almost similar mineral scaling experiments on bare and BSA-conditioned membranes were performed. These experiments all involved the following two or three steps: DI stabilization, organic conditioning (only for BSA conditioning membranes), and calcium sulfate scaling. First, a new bare membrane (ESPA-2, Hydranautics Inc.) was placed into the RO cell and stabilized by passing DI water, which took around 1 h. Second, a concentration of 60 mg/L of BSA solution was used for conditioning as a moderate-level concentration compared to other studies. In previous studies, the reported concentration of BSA varied from 3 mg/L to10 g/L, with the majority of the studies using a concentration ranging from 3 to 200 mg/L to investigate the effect of organic fouling on gypsum scaling.[8,11,12,26] In our study, we selected 60 mg/L to avoid clogging the membranes as observed with higher BSA concentrations and because our goal was to just condition the surface of the membranes. Furthermore, in our study, to easily control the fouling kinetics during membrane conditioning, the

https://doi.org/10.1021/acs.est.1c04143
Environ. Sci. Technol. XXXX, XXX, XXX−XXX

flow time of BSA solution was around 1.5−2 h, the membrane flux slightly decreased by around 5% for each triplicate membrane compared to their initial bare membrane permeate flux before BSA fouling, respectively. This procedure was carried out to prevent a significant flux decline compared to the control membranes and to obtain a very thin coating with the BSA biomolecules.[12,27] It should be noted that the 5% reduction in permeate flux was performed individually for each membrane to take into consideration membrane variability in each batch. However, we ensured that this 5% reduction, when it was averaged out with the three replicates, the membrane permeate flux was not statistically different from the bare membranes (Figure S9A). In that case, it allowed for an unbiased comparison of the bare and BSA-conditioned membranes in the subsequent scaling experiments. In addition, membrane characterizations were performed to ensure successful membrane conditioning with BSA using attenuated total reflection Fourier-transform infrared spectroscopy (ATR-FTIR, Digilab FTS 7000), scanning electron microscopy (Nova NanoSEM 230), and AFM (Innova, Bruke Inc.) (Text S2, Figures S1−S3). In the case of the scaling experiments on bare membranes, the step with BSA conditioning was skipped. Then, calcium sulfate scaling experiments on bare membranes were conducted for 1 h with the first solution condition (Table 1) and for 0.5 h with the second solution condition (Table 1), respectively. To figure out the correlation between the masses of mineral precipitates and the permeability of the membrane, calcium sulfate scaling experiments on BSA-conditioned membranes were performed until their final membrane permeability reached a similar level to that of bare membranes under both solution conditions.

2.3. Characterization Methods of Scalants on the Membranes. *2.3.1. Quantification of Mineral Precipitates on Membrane Surfaces.* For the first set of experiments, once the calcium sulfate scaling process on bare and BSA-conditioned membranes finished, the salt solution was switched to DI water, and the membranes were rinsed for 1 min to remove loosely attached calcium ions on the membrane. It should be noted that the rinsing was different from previously reported membrane cleaning procedures[13] because the cross-flow velocity for the membrane rinsing was decreased to 4.5 cm/s by lowering the pump speed, thus preventing any washing away of the precipitates. After that, the scaled membranes were removed from the membrane cell and air-dried and were then immersed in 50 mL hydrochloric acid [HCl, 0.5 (v/v %)] solution until the precipitates on the membranes were completely dissolved. The dissolved Ca concentrations were measured with AAS (AAnalyst 200, PerkinElmer Inc.). Triplicate membrane samples were used for each condition to quantify the calcium ion concentration.

2.3.2. Crystallinity and Morphology Characterizations of Mineral Precipitate on Membrane Surfaces. The other set of experiments were designed to investigate the crystallinity and three-dimensional topology of the mineral precipitates on the membrane surface. This set of experiments was very similar to the first one, except for the final step. The rinsing operation was skipped after the calcium sulfate scaling process. The fouled membranes were immediately taken out and air-dried. The crystallinity and the morphology of mineral precipitates were characterized with XRD (miniflex600, Rigaku) and VSI (NewView 7300, Zygo). Here, VSI could measure the morphology and the height of mineral precipitates on the membrane surface simultaneously. During VSI measurements, the height images were collected within the scanning depth of 200 μm. Each membrane sample was measured at five different spots. The height information was obtained through the analysis of Gwyddion (release 2.53, gwyddion.net). The average height of the mineral crystals was reported through a statistical analysis of 30 crystals at five different observation spots for each membrane sample.

To investigate the height changes of mineral precipitates on both membranes over time, an additional set of calcium sulfate scaling experiments for different time periods including 0.5, 1, 2 3, and 6 h, were conducted on bare and BSA-conditioned membranes under the first solution condition (Table 1). After the scaling process was finished, the scaled membranes were air-dried and observed using VSI with the same measurement methods as described above.

2.4. GIWAXS Measurements of Mineral Precipitates on the Membrane and on the Organic Surface. To serve as a supplementary experiment, GIWAXS measurements (beam-line 12 ID-B at advanced photon source (APS), Argonne National Laboratory) were used to characterize the crystallinity of mineral precipitates at the initial stage on bare and BSA-conditioned membranes. The detection of the mineral phase using XRD was limited due to the low amount of precipitates formed at the beginning of the runs in the RO system. Therefore, calcium sulfate scaling tests on bare and BSA-conditioned membranes in a batch system were conducted. To mimic the local environment on the membrane surface, batch reactions were conducted under an SI of 0.17, which is the local saturation index (Table 1. Bulk SI_{gyp} = 0.07, Local SI_{gyp} = 0.17) on the membrane surface. After soaking the bare and BSA-conditioned membranes into calcium sulfate solutions for 5 min, both membranes were taken out, rinsed with ethanol, and finally dried with a stream of nitrogen. Duplicate samples were prepared and each sample was measured at three different spots. Before GIWAXS measurements, the membrane samples were aligned to be parallel to the incident X-ray beam. The energy of the synchrotron X-ray radiation was 13.3 keV. GIWAXS patterns were recorded at an X-ray incidence angle of 0.1° with an exposure time of 1 s.[28]

To investigate the influences of different functional groups on crystallinity, similar batch experiments of calcium sulfate precipitation with diverse functional groups terminated self-assembled monolayers (SAMs) were performed including COOH terminated, and mixed NH_2&COOH terminated organic coatings. The precipitates on the SAMs coatings were similarly examined using GIWAXS. More measurement details are presented in the Supporting Information (Text S3).

2.5. Ex Situ AFM Measurements of Calcium Sulfate Precipitates on Polyamide Films. Besides VSI measurements, ex situ AFM measurements were also used to observe the nano-scale topology of mineral precipitates on polyamide films. Due to the interference of the membrane surface roughness, it was very challenging to observe the growth mechanisms of calcium sulfate precipitates. Hence, polyamide films were coated on a silica wafer using a spin-assisted molecular layer-by-layer (mLbL) deposition technique. The synthesis method is described in the Supporting Information (Text S4) and previous publications.[29,30] For the experiment, the polyamide films were immersed in a calcium sulfate solution with an SI of 0.17 overnight. The precipitated films were rinsed using deionized water and dried with nitrogen before the measurement. Then, the tapping mode was employed to scan the polyamide surfaces using a scan rate of

https://doi.org/10.1021/acs.est.1c04143
Environ. Sci. Technol. XXXX, XXX, XXX−XXX

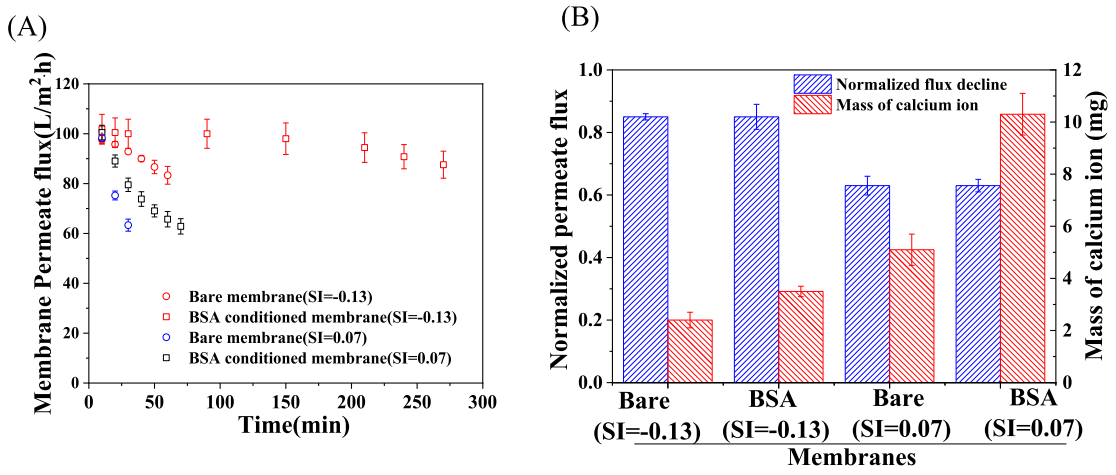

Figure 1. (A) Membrane permeate flux of bare and BSA-conditioned membranes after gypsum scaling over time under two different solution conditions (bulk SI_{gyp} = −0.13, and 0.07); (B) mass of calcium ion measured by dissolving calcium sulfate precipitates on bare and BSA-conditioned membranes with the same normalized membrane flux under two solution conditions. The normalized permeate flux in the *Y*-axis was normalized by the initial membrane permeate flux in the scaling experiment.

0.5 Hz. The height, amplitude, and phase images were collected simultaneously and processed using NanoScope Analysis 1.5.

3. RESULTS AND DISCUSSION

3.1. Uncorrelated Relationship between the Amount of Mineral Precipitates and the Permeability Decay of the Membrane. Figure 1A shows the membrane permeate flux of calcium sulfate scaling on bare and BSA-conditioned membranes under two solution conditions (Table 1). Under both solution conditions, the membrane flux decay rate of the bare membrane was much faster than the BSA-conditioned membrane (Figure 1A). For example, under solution condition 1, the permeability of bare and BSA-conditioned membranes decreased by 85 ± 1% (Figure 1B-normalized flux, Figure S9-non-normalized flux) in 60 and 270 min, respectively (Figure 1A). Under solution condition 2, due to the accelerated surface crystallization rate caused by the higher saturation index (SI = 0.07), the permeability of bare and BSA-conditioned membranes was controlled to decrease by 63 ± 2% (Figure 1B-normalized flux, Figure S9-non-normalized flux) in 30 and 70 min, respectively (Figure 1A).

Previous studies indicated that the slower permeability decay on BSA-conditioned membrane was due to changes in membrane surface properties after BSA conditioning (i.e., surface charge, increase in carboxyl group density, the interaction of forces, and so forth).[8,11,12,31] Our membrane surface characterizations of bare and BSA-conditioned membranes confirmed some of these changes. BSA-conditioned membranes exhibited more hydrophobicity and less negative zeta potential than the bare membranes (Table S1). In addition, Liu and Mi observed that HA and SA-fouled membranes had a different scaling behavior than BSA-fouled membranes, they hypothesized that the governing gypsum scaling mechanisms on BSA-fouled membranes were likely dependent on the combined effects of various factors, possibly carboxyl group density and a biomolecule structure.[12] Wang et al. demonstrated that the average adhesive forces of gypsum-BSA-fouled membranes were less than those of gypsum-virginal membranes, resulting in a relatively higher energy barrier for gypsum nucleation on BSA-fouled membranes and hence a reduced permeate flux decline.[8]

Besides the inhibited permeability decay in the presence of BSA, those studies also demonstrated that conditioning with different organic molecules can affect the morphology of gypsum precipitates.[8,11,12] For example, in Wang's study, gypsum crystals on bare membranes and BSA-fouled presented a plate-like and rod-like shape, respectively; while needle and serried crystals were observed on HA-fouled and SA-fouled membranes, respectively.[8] Because none of these previous studies fully characterized the amount, growth orientation, and crystallinity of the mineral precipitates, it is still unclear their roles in controlling the permeability of the membrane. From these studies, the following question was raised: is the permeability decline controlled by the amount or by the morphology of mineral precipitates?

To answer to this knowledge gap, the masses of calcium sulfate precipitates on bare and BSA-conditioned membranes were quantified (Figure 1B). Prior studies hypothesized that the permeability decline of the membrane was positively related to the amount of deposited precipitates on the membrane surface.[32−34] Interestingly, even though bare and BSA-conditioned membranes reduced to the same permeability, the masses of calcium sulfate precipitates (Figure 1B) on BSA-conditioned membranes were around two times more than those on bare membranes under both solution conditions. Moreover, these quantification results indicated that the masses of calcium sulfate precipitates on the membrane did not correlate with the permeability of the membrane. Hence, we can conclude that the masses of mineral precipitates cannot solely explain the permeability decay of the membranes.

3.2. Effects of Distinct Growth Behaviors of Mineral Precipitates on Bare and BSA-Conditioned Membranes on Membrane Permeability. Rahardianto et al. found that the permeability decline did not correlate exactly to the surface area coverage by scaling. They hypothesized that it was due to the three-dimensional structure of the rosette-like gypsum and suggested that only the base of the gypsum rosette was in close contact with the membrane, which affected the membrane permeability.[23] Similarly, Shaffer et al. demonstrated that besides the base of gypsum rosette, their loose branches could allow the permeate to get through.[10] These previous studies

https://doi.org/10.1021/acs.est.1c04143
Environ. Sci. Technol. XXXX, XXX, XXX−XXX

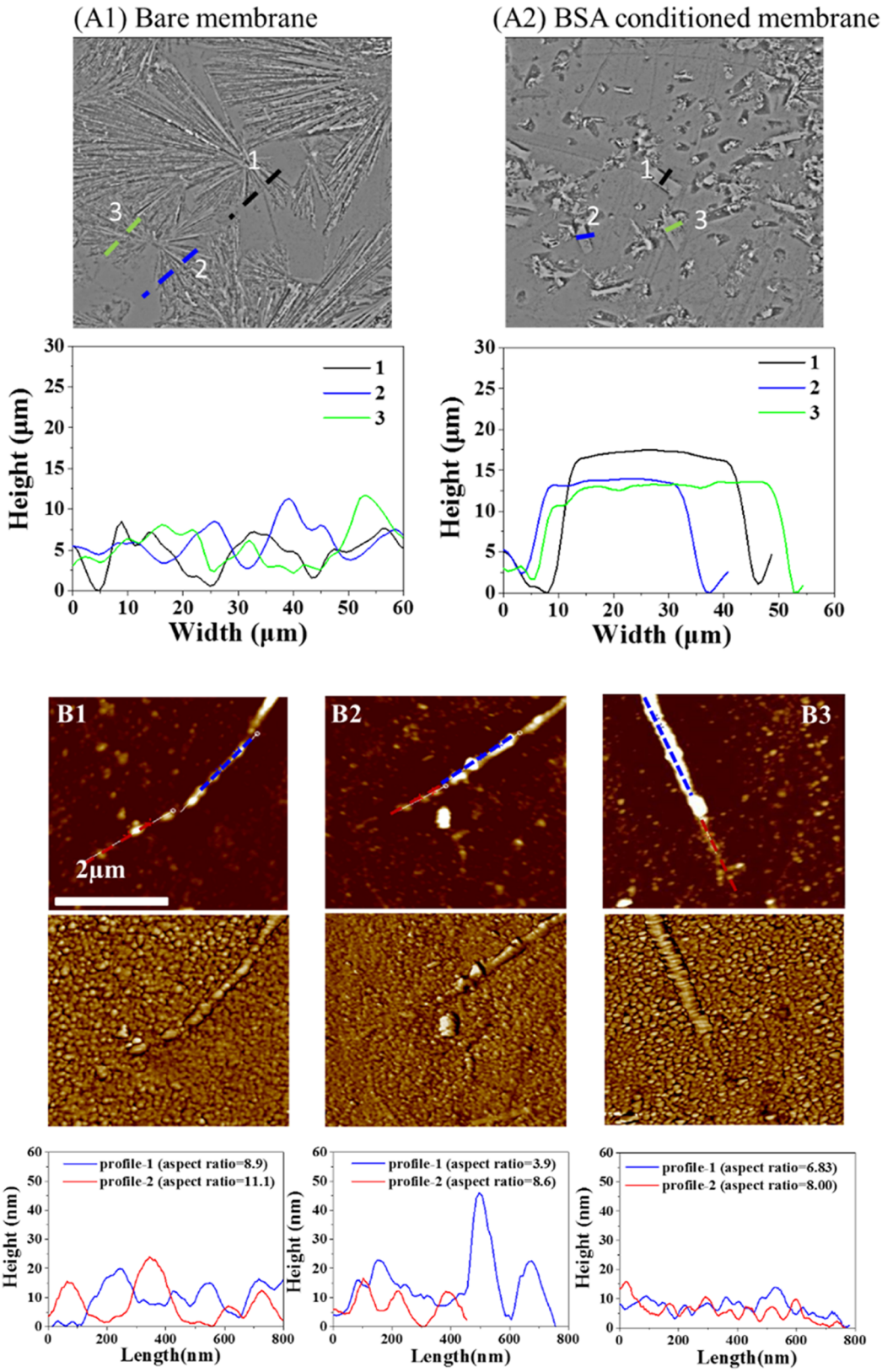

Figure 2. VSI observations and height profiles of gypsum crystals on bare (A1) and BSA-conditioned membranes (A2) under the solution condition 1. The height profiles below the VSI images show the height of gypsum crystals along the dashed lines. Replicate measurement results (B1−B3) by AFM tapping-mode of calcium sulfate precipitates on polyamide films after 24 h batch precipitation tests. The scan size is 2 μm × 2 μm, and the height scale is 30 nm. These tapping phase images present the growth mechanism of the needle-like crystals. The height profiles under the AFM images show the height of the needle crystal on polyamide films along the red and blue dashed lines. The aspect ratio (length/height) for each cut line was calculated.

https://doi.org/10.1021/acs.est.1c04143
Environ. Sci. Technol. XXXX, XXX, XXX−XXX

hypothesized that the permeate flux decline was somehow linked to the morphology of gypsum crystals, suggesting that the structures of mineral scales could play a role in the permeability of the membrane.

To confirm this hypothesis, the morphologies and heights of precipitates on bare and BSA-conditioned membranes were observed using VSI as shown in Figure 2 (A1, A2). The precipitates on BSA-conditioned membranes [Figure 2 (A2)] presented a rod-like shape, which was different from the rosette-like structure on bare membranes [Figure 2 (A1)]. This finding was consistent with the morphology of gypsum crystals on BSA-conditioned membranes reported by prior studies.[8,11,12] In the case of bare membranes, our study showed similar results to the study by Shih et al. where it was observed that needle-like crystals on bare membranes tend to radiate out from a center of the gypsum cluster at the membrane surface.[35] Furthermore, the height profile in our study [Figure 2 (A1)] showed that each branch of the rosette structure had a similar height but was markedly thinner than the rod-like crystals on BSA-conditioned membranes. To reveal the height changes of the crystal over time, calcium sulfate scaling on bare and BSA-conditioned membranes in a time series was also conducted. As depicted in Figure 3, the height of the crystals on bare

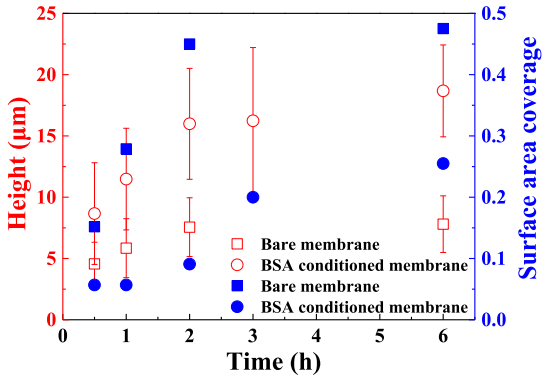

Figure 3. Time series under the solution condition 1 (Bulk SI_{gyp} = −0.13, Local SI_{gyp} = 0.02) during calcium sulfate scaling on bare and BSA-conditioned membranes. Measurements of the height and surface area coverage of mineral crystals on bare and BSA-conditioned membranes versus time. The height of the crystals obtained from VSI observations was determined by statistical analysis (30 crystals from five observation spots for each membrane sample). The surface coverage of mineral precipitates, the ratio of the coverage area of precipitates and original membrane area, were determined using the surface blockage model.

membranes during 6-h scaling varied less than those on BSA-conditioned membranes, and the height of the crystals on BSA-conditioned membranes was apparently greater than that on bare membranes. These results demonstrated that the crystals on BSA-conditioned membranes were likely to grow thicker, and had a lower surface area coverage of precipitates on the membrane.

To link the height of the crystals with the permeate flux decline of the membrane, the surface blockage model (Text S5) was used to determine the surface area coverage of the precipitates.[32] As described by the model, the growing crystals could gradually block the membrane surface and reduce the effective area for permeation, resulting in a permeate flux decline. Before that, the applicability of the model for our current system was validated. The model validation results, presented in the Supporting Information (Text S6), confirmed that the surface blockage model was applicable to our current system. On the basis of the model, the surface area coverage of precipitates on the membrane was related to the normalized permeate flux at the end of the scaling process (details in Text S5). Figure 3 also shows that at the initial scaling stage (0−2 h), the surface area coverage of the precipitates on bare membranes increased faster than that for BSA-conditioned membranes. It should be mentioned that the surface area coverage on bare membranes eventually reached a plateau after a rapid increment, while for BSA-conditioned membranes, the surface area coverage kept increasing gradually and took longer (more than 2 h) to reach a plateau (Figure 3), indicating that the BSA on the membrane affected crystal growth. Hence, we hypothesized that the differences in surface area coverage of precipitates on bare and BSA-conditioned membranes were probably linked to the oriented growth of the crystal on the membrane.

Tapping mode AFM measurements on polyamide films were further performed to confirm the hypothesis [Figures 2 (B1−B3), and S6]. Those AFM images exhibited oriented aggregates at the end of the needle-like crystals (their growth direction). Additionally, the enhanced trend of aspect ratios of the needle crystals suggested that the increasing oriented aggregation extent was occurring from the newest growing ends. This finding was consistent with previous studies, which demonstrated that needle gypsum crystals in bulk aqueous solutions were formed from the oriented attachment of nanobassanite.[18,19,36,37] Christie et al. also reported that the oriented growth of gypsum during membrane distillation was able to easily cover the membrane surface, eventually compromising the distillate quality.[38] In our case, the oriented aggregation-based growth of needle-like crystals on the polyamide film led to larger surface area coverage of precipitates on the bare membrane, thus aggravating the loss of membrane permeability.

To our knowledge, this is the first study where direct nanoscale observations were performed and demonstrated that the oriented aggregation of $CaSO_4$ nanoparticles produced needle-like crystals on the polyamide films. In the case of BSA-conditioned membranes, a thick rod-like crystal was formed, which did not markedly result in a large surface area coverage such as the needle-like crystals. Therefore, in the case of the BSA-conditioned membranes, longer RO runs were necessary to obtain the same membrane flux decline as the bare membranes (Figures 1B and S9). These long runs led to a larger mass of Ca ions incorporated into the precipitates to reach the same surface area coverage as bare membranes. As such, these findings have a significant implication on the mitigation of membrane flux decline caused by scaling. These results also suggest that controlling the growth orientation of gypsum crystals on the RO membranes can affect the membrane permeability decay.

3.3. Roles of BSA in Controlling the Morphology of Mineral Precipitates on Membranes. To gain deep insights into the role of crystallinity in the different crystal growth orientations observed in Figure 2, the mineral phases of the crystals formed on both types of membranes after different scaling periods were analyzed using GIWAXS and XRD, respectively. GIWAXS measurements were performed to characterize the crystallinity of calcium sulfate precipitates at the initial scaling stage (5 min). Figure 4 shows that the characteristic peak of gypsum at q = 0.82 was present on both

https://doi.org/10.1021/acs.est.1c04143
Environ. Sci. Technol. XXXX, XXX, XXX−XXX

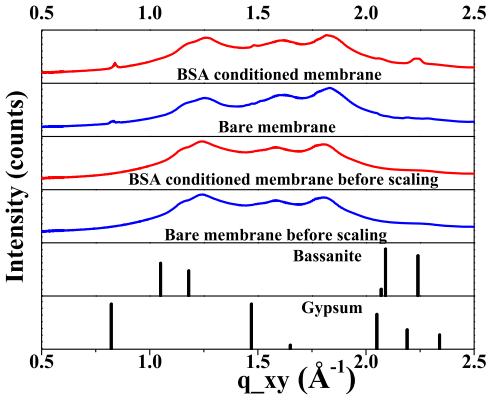

Figure 4. GIWAXS measurements of mineral precipitates on bare and BSA-conditioned membranes in a batch system under the SI of 0.17 mimicking the local SI on the membrane surface (solution condition 2).

bare and BSA-conditioned membranes, while the characteristic peak of bassanite at q = 2.25 was only observed on BSA-conditioned membranes, indicating that BSA could stabilize bassanite, which is a precursor for gypsum formation.[19−21,36,37,39−41] This finding was consistent with the studies by Aizenberg et al.,[42,43] where organic macromolecules with abundant carboxylic functional groups could stabilize the transition of amorphous $CaCO_3$ to crystalline calcite, thus affecting the growth orientation of crystals because amorphous materials are isotropic and moldable and can easily overcome the directional restrictions of crystals.[44] Based on the literature, top (111) crystal facets of bassanite are enriched in Ca^{2+} ions, any interactions with Ca (II) of the bassanite facets can inhibit oriented growth along the c-axis to form needle-like gypsum crystals.[18] Therefore, it is suggested that these (111) crystal facets found on the bassanite might have been inhibited or blocked on the BSA-conditioned membrane, which would explain why their membrane surfaces presented a rod-shaped structure rather than a needle-like structure. Once the disruption of oriented growth of the crystal happened, the amorphous bassanite served as a template for crystal thickening as they have energetically favorable interfaces for Ca incorporation due to the roughened interfaces with a higher density of kink sites.[45,46] These factors might explain the effect of bassanite and BSA on the orientation of the scaling on the membrane discussed earlier.

In addition to GIWAXS measurements at the initial crystal growth steps, XRD was also used to analyze the mineral phase, and crystallographic orientations of the precipitates on both membranes at the end of the relatively longer RO run. As indicated in Figure S7, gypsum was identified as the main mineral phase on bare and BSA-conditioned membranes under both solution conditions. The presence of gypsum on both membranes suggested that bassanite observed in the GWAXS measurement was eventually converted to gypsum, which indicated that the BSA conditioning layer can temporarily delay the conversion of bassanite to gypsum. In addition, under the solution condition 1, the diffraction peak intensity of (020) crystal facets on the bare membrane was stronger than the other facets, while for BSA-conditioned membranes, the (041) crystal facets had a higher diffraction intensity in contrast to the other facets (Figure S7). These differences in crystallographic orientations can further validate the observed morphological changes of gypsum crystals as discussed earlier. Such differences were attributed to the varying growth rates of different crystal facets.[47−51] In our case, the (020) crystal facet on the bare membrane seemed to be the preferred direction for the crystal growth, while for the BSA membrane, it was the (041) crystal facet, which led to differences in crystal growth orientations and morphologies between both membranes.

To figure out the reason for organic macromolecules, such as BSA, with abundant carboxylic functional groups being able to stabilize the transition from bassanite to gypsum, we also performed GIWAXS measurements of calcium sulfate precipitates on COOH-terminated and the mixed NH_2&COOH-terminated SAMs. This assumption was based on previous investigations where organic additives, including organic inhibitors (polyacrylic acid), carboxylic acids (tartaric, maleic, and citric acids) have been shown to retard the phase transition from bassanite to gypsum.[18,21,41,52] The results (Figure S8) in our study confirmed that the stabilization of bassanite preferentially occurred on SAMs with carboxylic functional groups (−COOH). Based on the surface density of −COOH measured by the toluidine blue O colorimetric method (Text S2), BSA coatings (0.33 ± 0.01 $\mu g/cm^2$) had a statistically significantly higher (unpaired two-tailed, p = 0.0023) density of −COOH than polyamide RO membrane (0.22 ± 0.03 $\mu g/cm^2$). This difference together with the BSA molecular structure and its other functional groups might have contributed to the stabilization of bassanite and the change of crystal morphology on BSA-conditioned membranes. In the case of the molecular structure, BSA molecules have been shown to have structural flexibility due to the existence of Gly residues, which can affect the crystal growth process.[53−55] Similar to the finding by Xue et al., BSA molecular chains also contain amino acids, which have varied functional groups including −COOH (i.e. aspartic acid, glutamic acid), −OH, and −SH (i.e., serine, cysteamine, and lysine, and so forth), which can also provide enough sites for the binding of bassanite, and hence stabilize it at an extended timescale as revealed by the GIWAXS measurements.[55] In addition to the −COOH functional group, gypsum presents doublet absorption peaks at 1686 and 1623 cm^{-1} that are assigned to the ν_2 water bending mode, while the ν_2 water bending mode only exists at 1623 cm^{-1} for bassanite.[40,56] As indicated in FTIR spectra (Figure S10), except gypsum, only the spectra for BSA-conditioned membranes after scaling with 5 min exhibited the ν_2 water bending mode at 1623 cm^{-1}, while after a longer scaling run, both membranes exhibited the doublet absorption peaks of gypsum, which suggested that a H_2O molecule within the crystal structure could be another reason for the stabilization of bassanite. This observation has also been mentioned in the study by Yin et al.[57] where the release of H_2O adsorbed to Ca (II) as a result of ligand exchange between −COO− of BSA molecule and −OH of H_2O within the $CaSO_4$ can result in the capability of BSA molecules in preventing the transformation of amorphous bassanite to gypsum crystal.[58,59] Furthermore, it was previously observed that the stabilization of bassanite disrupted the oriented growth of gypsum crystals, leading to the subsequent growth along (041) crystal facets on the BSA-coated membrane rather than the (020) crystal facet as described in detail during the XRD analysis. Hence, rod-like gypsum crystals on BSA-coated membranes were formed as opposed to the needle-like crystals on bare membranes.

https://doi.org/10.1021/acs.est.1c04143
Environ. Sci. Technol. XXXX, XXX, XXX−XXX

4. ENVIRONMENTAL IMPLICATIONS

Due to the high-sulfate content in seawater or brackish water, gypsum formation during membrane desalination will impair the membrane permeability without any treatment.[6] Furthermore, the ubiquitous existence of biomolecules (i.e., proteins, such as BSA) in natural water have been previously suggested to affect membrane scaling.[8,11,12,27] Here, different experimental conditions mimicking brackish water were used to study gypsum scaling on RO desalination.[23] In this study, we have demonstrated that more mass of mineral precipitates occurred on BSA-conditioned membranes than bare membranes; however, the membrane permeability decline was slower for BSA-conditioned membranes than for bare membranes. This phenomenon was attributed to the differences in growth orientation of gypsum crystals on both types of membranes. This slow membrane flux decline rate corroborates that biomolecules do not inhibit scaling but do not necessarily aggravate the effects of scaling. In fact, the difference in carboxylic density between BSA-conditioned membrane and bare membrane, together with the structure and other functional groups of the BSA molecule, played a role in the stabilization of bassanite and disruption of oriented growth of gypsum crystals, thus alleviating the scaling effect on membrane permeability decay. This finding has improved our fundamental understanding of the crystallization mechanism of mineral scaling in the presence of biomolecules. Also, it suggested that the membrane scaling formation can be controlled by stabilizing the scale precursor, thus alleviating the detrimental effect of scaling on the RO membrane flux and ultimately increasing the membrane lifespan.[57] Hence, this study could guide a more tailored molecular design of scaling-resistant coatings to increase the usability of the membrane for a longer time. Furthermore, regarding macromolecules in the natural water, future studies combining biomolecule fouling and scaling studies should be pursued to optimize the macromolecule control strategies. Because the biomolecule fouling and scaling still pose threat to the performance of membrane desalination, a good pre-treatment procedure design before RO operations could effectively control the organic and mineral fouling as well as lower the operational costs.

■ ASSOCIATED CONTENT

Supporting Information

The Supporting Information is available free of charge at https://pubs.acs.org/doi/10.1021/acs.est.1c04143.

Experimental details and results, characterization results of bare and BSA-conditioned membranes, surface blockage model description and validation, and synthesis method of polyamide films (PDF)

■ AUTHOR INFORMATION

Corresponding Authors

Debora F. Rodrigues − *Department of Civil and Environmental Engineering, University of Houston, Houston, Texas 77004, United States;* orcid.org/0000-0002-3124-1443; Phone: (713)743-4285; Email: dfrigirodrigues@uh.edu; Fax: 713-743-4260

Yandi Hu − *Department of Civil and Environmental Engineering, University of Houston, Houston, Texas 77004, United States; Department of Environmental Science and Engineering, Peking University, Beijing 100871, China;* Phone: 713-743-1495; Email: huyandi@pku.edu.cn; Fax: 713-743-4260

Authors

Meng Wang − *Department of Civil and Environmental Engineering, University of Houston, Houston, Texas 77004, United States*

Bo Cao − *Department of Civil and Environmental Engineering, University of Houston, Houston, Texas 77004, United States*

Complete contact information is available at: https://pubs.acs.org/10.1021/acs.est.1c04143

Author Contributions

§Y.H. and D.F.R. contributed equally to this work

Notes

The authors declare no competing financial interest.

■ ACKNOWLEDGMENTS

This study is based upon work supported by the National Science Foundation under grant no. CHE-1904472. We highly appreciate Dr. Xiaobing Zuo for GIWAXS measurements, and the use of facilities at the beamline sector of 12-ID-B, APS, Argonne National Laboratory. Use of beamlines was supported by the US Department of Energy, Office of Basic Energy Science, under contract no. DE-AC02-06CH11357.

■ REFERENCES

(1) Energy, D.; Elimelech, M.; Phillip, W. A. The Future of Seawater and the Environment. *Science 80* **2011**, *333*, 712−717.

(2) Schiermeier, Q. Water: A long dry summer. *Nature* **2008**, *452*, 270−273.

(3) Greenlee, L. F.; Lawler, D. F.; Freeman, B. D.; Marrot, B.; Moulin, P. Reverse Osmosis Desalination: Water Sources, Technology, and Today's Challenges. *Water Res.* **2009**, *43*, 2317−2348.

(4) Antony, A.; Low, J. H.; Gray, S.; Childress, A. E.; Le-Clech, P.; Leslie, G. Scale Formation and Control in High Pressure Membrane Water Treatment Systems: A Review. *J. Membr. Sci.* **2011**, *383*, 1−16.

(5) Matin, A.; Rahman, F.; Shafi, H. Z.; Zubair, S. M. Scaling of Reverse Osmosis Membranes Used in Water Desalination : Phenomena , Impact , and Control ; Future Directions. *Desalination* **2019**, *455*, 135−157.

(6) Tong, T.; Wallace, A. F.; Zhao, S.; Wang, Z. Mineral Scaling in Membrane Desalination : Mechanisms , Mitigation Strategies , and Feasibility of Scaling-Resistant Membranes. *J. Membr. Sci.* **2019**, *579*, 52−69.

(7) Yan, Z.; Qu, F.; Liang, H.; Yu, H.; Pang, H.; Rong, H.; Fan, G.; Van der Bruggen, B. Effect of Biopolymers and Humic Substances on Gypsum Scaling and Membrane Wetting during Membrane Distillation. *J. Membr. Sci.* **2021**, *617*, 118638.

(8) Wang, J.; Wang, L.; Miao, R.; Lv, Y.; Wang, X.; Meng, X.; Yang, R.; Zhang, X. Enhanced Gypsum Scaling by Organic Fouling Layer on Nanofiltration Membrane: Characteristics and Mechanisms. *Water Res.* **2016**, *91*, 203−213.

(9) Karabelas, A. J.; Karanasiou, A.; Sioutopoulos, D. C. Experimental Study on the Effect of Polysaccharides on Incipient Membrane Scaling during Desalination. *Desalination* **2017**, *416*, 106−121.

(10) Shaffer, D. L.; Tousley, M. E.; Elimelech, M. Influence of Polyamide Membrane Surface Chemistry on Gypsum Scaling Behavior. *J. Membr. Sci.* **2017**, *525*, 249−256.

(11) Benecke, J.; Rozova, J.; Ernst, M. Anti-Scale Effects of Select Organic Macromolecules on Gypsum Bulk and Surface Crystallization during Reverse Osmosis Desalination. *Sep. Purif. Technol.* **2018**, *198*, 68−78.

(12) Liu, Y.; Mi, B. Effects of Organic Macromolecular Conditioning on Gypsum Scaling of Forward Osmosis Membranes. *J. Membr. Sci.* **2014**, *450*, 153−161.
(13) Baoxia, M.; Elimelech, M. Gypsum Scaling and Cleaning in Forward Osmosis: Measurements and Mechanisms. *Environ. Sci. Technol.* **2010**, *44*, 2022−2028.
(14) Cao, B.; Ansari, A.; Yi, X.; Rodrigues, D. F.; Hu, Y. Gypsum Scale Formation on Graphene Oxide Modified Reverse Osmosis Membrane. *J. Membr. Sci.* **2018**, *552*, 132−143.
(15) Ansari, A.; Peña-Bahamonde, J.; Wang, M.; Shaffer, D. L.; Hu, Y.; Rodrigues, D. F. Polyacrylic Acid-Brushes Tethered to Graphene Oxide Membrane Coating for Scaling and Biofouling Mitigation on Reverse Osmosis Membranes. *J. Membr. Sci.* **2021**, *630*, 119308.
(16) Jaramillo, H.; Boo, C.; Hashmi, S. M.; Elimelech, M. Zwitterionic Coating on Thin-Film Composite Membranes to Delay Gypsum Scaling in Reverse Osmosis. *J. Membr. Sci.* **2021**, *618*, 118568.
(17) Singh, N. B.; Middendorf, B. Calcium Sulphate Hemihydrate Hydration Leading to Gypsum Crystallization. *Prog. Cryst. Growth Charact. Mater.* **2007**, *53*, 57−77.
(18) Tartaj, P.; Morales, J.; Fernández-DÍaz, L. CaSO4 Mineralization in Carboxy- and Amino-Functionalized Reverse Micelles Unravels Shape-Dependent Transformations and Long-Term Stabilization Pathways for Poorly Hydrated Nanophases (Bassanite). *Cryst. Growth Des.* **2015**, *15*, 2809−2816.
(19) Van Driessche, A. E. S.; Benning, L. G.; Rodriguez-Blanco, J. D.; Ossorio, M.; Bots, P.; García-Ruiz, J. M. The Role and Implications of Bassanite as a Stable Precursor Phase to Gypsum Precipitation. *Science 80* **2012**, *336*, 69−72.
(20) Stawski, T. M.; Van Driessche, A. E. S.; Ossorio, M.; Diego Rodriguez-Blanco, J.; Besselink, R.; Benning, L. G. Formation of Calcium Sulfate through the Aggregation of Sub-3 Nanometre Primary Species. *Nat. Commun.* **2016**, *7*, 11177.
(21) Wang, Y. W.; Meldrum, F. C. Additives Stabilize Calcium Sulfate Hemihydrate (Bassanite) in Solution. *J. Mater. Chem.* **2012**, *22*, 22055−22062.
(22) Le Gouellec, Y. A.; Elimelech, M. Calcium Sulfate (Gypsum) Scaling in Nanofiltration of Agricultural Drainage Water. *J. Membr. Sci.* **2002**, *205*, 279−291.
(23) Rahardianto, A.; Shih, W. Y.; Lee, R. W.; Cohen, Y. Diagnostic Characterization of Gypsum Scale Formation and Control in RO Membrane Desalination of Brackish Water. *J. Membr. Sci.* **2006**, *279*, 655−668.
(24) Zydney, A. L. Stagnant Film Model for Concentration Polarization in Membrane Systems. *J. Membr. Sci.* **1997**, *130*, 275−281.
(25) Sutzkover, I.; Hasson, D.; Semiat, R. Simple Technique for Measuring the Concentration Polarization Level in a Reverse Osmosis System. *Desalination* **2000**, *131*, 117−127.
(26) Ang, W. S.; Elimelech, M. Protein (BSA) Fouling of Reverse Osmosis Membranes: Implications for Wastewater Reclamation. *J. Membr. Sci.* **2007**, *296*, 83−92.
(27) Quay, A. N.; Tong, T.; Hashmi, S. M.; Zhou, Y.; Zhao, S.; Elimelech, M. Combined Organic Fouling and Inorganic Scaling in Reverse Osmosis: Role of Protein−Silica Interactions. *Environ. Sci. Technol.* **2018**, *52*, 9145−9153.
(28) Dai, C.; Zhao, J.; Giammar, D. E.; Pasteris, J. D.; Zuo, X.; Hu, Y. Heterogeneous Lead Phosphate Nucleation at Organic-Water Interfaces: Implications for Lead Immobilization. *ACS Earth Space Chem.* **2018**, *2*, 869−877.
(29) Tousley, M. E.; Shaffer, D. L.; Lee, J. H.; Osuji, C. O.; Elimelech, M. Effect of Final Monomer Deposition Steps on Molecular Layer-by-Layer Polyamide Surface Properties. *Langmuir* **2016**, *32*, 10815−10823.
(30) Chan, E. P.; Lee, J.-H.; Chung, J. Y.; Stafford, C. M. An Automated Spin-Assisted Approach for Molecular Layer-by-Layer Assembly of Crosslinked Polymer Thin Films. *Rev. Sci. Instrum.* **2012**, *83*, 114102.
(31) Mi, B.; Elimelech, M. Chemical and Physical Aspects of Organic Fouling of Forward Osmosis Membranes. *J. Membr. Sci.* **2008**, *320*, 292−302.
(32) Gilron, J.; Hasson, D. Calcium Sulphate Fouling of Reverse Osmosis Membranes: Flux Decline and Mechanism. *Chem. Eng. Sci.* **1987**, *42*, 2351−2360.
(33) Brusilovsky, M.; Borden, J.; Hasson, D. Flux Decline Due to Gypsum Precipitation on RO Membranes. *Desalination* **1992**, *86*, 187−222.
(34) Borden, J.; Gilron, J.; Hasson, D. Analysis Of Ro Flux Decline Due To Membrane Surface Blockage. *Desalination* **1987**, *66*, 257−269.
(35) Shih, W. Y.; Rahardianto, A.; Lee, R. W.; Cohen, Y. Morphometric Characterization of Calcium Sulfate Dihydrate (Gypsum) Scale on Reverse Osmosis Membranes. *J. Membr. Sci.* **2005**, *252*, 253−263.
(36) Saha, A.; Lee, J.; Pancera, S. M.; Bräeu, M. F.; Kempter, A.; Tripathi, A.; Bose, A. New Insights into the Transformation of Calcium Sulfate Hemihydrate to Gypsum Using Time-Resolved Cryogenic Transmission Electron Microscopy. *Langmuir* **2012**, *28*, 11182−11187.
(37) Wang, Y. W.; Kim, Y. Y.; Christenson, H. K.; Meldrum, F. C. A New Precipitation Pathway for Calcium Sulfate Dihydrate (Gypsum) via Amorphous and Hemihydrate Intermediates. *Chem. Commun.* **2012**, *48*, 504−506.
(38) Christie, K. S. S.; Yin, Y.; Lin, S.; Tong, T. Distinct Behaviors between Gypsum and Silica Scaling in Membrane Distillation. *Environ. Sci. Technol.* **2020**, *54*, 568−576.
(39) He, K.; Nie, A.; Yuan, Y.; Ghodsi, S. M.; Song, B.; Firlar, E.; Lu, J.; Lu, Y.; Shokuhfar, T.; Megaridis, C. M.; Shahbazian-Yassar, R. In Situ Transmission Electron Microscopy Explores a New Nanoscale Pathway for Direct Gypsum Formation in Aqueous Solution. *ACS Appl. Nano Mater.* **2018**, *1*, 5430−5440.
(40) Jones, F. Infrared Investigation of Barite and Gypsum Crystallization: Evidence for an Amorphous to Crystalline Transition. *CrystEngComm* **2012**, *14*, 8374−8381.
(41) Rabizadeh, T.; Peacock, C. L.; Benning, L. G. Carboxylic Acids: Effective Inhibitors for Calcium Sulfate Precipitation? *Mineral. Mag.* **2014**, *78*, 1465−1472.
(42) Aizenberg, J.; Lambert, G.; Weiner, S.; Addadi, L. Factors Involved in the Formation of Amorphous and Crystalline Calcium Carbonate:A Study of an Ascidian Skeleton. *J. Am. Chem. Soc.* **2002**, *124*, 32−39.
(43) Aizenberg, J.; Addadi, L.; Weiner, S.; Lambert, G. Stabilization of Amorphous Calcium Carbonate by Specialized Macromolecules in Biological and Synthetic Precipitates. *Adv. Mater.* **1996**, *8*, 222−226.
(44) Nudelman, F.; Sommerdijk, N. A. J. M. Biomineralization as an Inspiration for Materials Chemistry. *Angew. Chem., Int. Ed.* **2012**, *51*, 6582−6596.
(45) Chung, J.; Taylor, M. G.; Granja, I.; Asplin, J. R.; Mpourmpakis, G.; Rimer, J. D. Factors Differentiating the Effectiveness of Polyprotic Acids as Inhibitors of Calcium Oxalate Crystallization in Kidney Stone Disease. *Cryst. Growth Des.* **2018**, *18*, 5617−5627.
(46) Xie, B.; Nancollas, G. H. How to Control the Size and Morphology of Apatite Nanocrystals in Bone. *Proc. Natl. Acad. Sci. U.S.A.* **2010**, *107*, 22369−22370.
(47) Liu, S. T.; Nancollas, G. H. A Kinetic and Morphological Study of the Seeded Growth of Calcium Sulfate Dihydrate in the Presence of Additives. *J. Colloid Interface Sci.* **1975**, *52*, 593−601.
(48) Rabizadeh, T.; Stawski, T. M.; Morgan, D. J.; Peacock, C. L.; Benning, L. G. The Effects of Inorganic Additives on the Nucleation and Growth Kinetics of Calcium Sulfate Dihydrate Crystals. *Cryst. Growth Des.* **2017**, *17*, 582−589.
(49) Mbogoro, M. M.; Peruffo, M.; Adobes-Vidal, M.; Field, E. L.; O'Connell, M. A.; Unwin, P. R. Quantitative 3D Visualization of the Growth of Individual Gypsum Microcrystals: Effect of Ca^{2+}:SO_4^{2-} Ratio on Kinetics and Crystal Morphology. *J. Phys. Chem. C* **2017**, *121*, 12726−12734.

https://doi.org/10.1021/acs.est.1c04143
Environ. Sci. Technol. XXXX, XXX, XXX−XXX

(50) Montagnino, D.; Costa, E.; Massaro, F. R.; Artioli, G.; Aquilano, D. Growth Morphology of Gypsum in the Presence of Copolymers. *Cryst. Res. Technol.* **2011**, *1018*, 1010−1018.
(51) Mao, X.; Song, X.; Lu, G.; Xu, Y.; Sun, Y.; Yu, J. Effect of Additives on the Morphology of Calcium Sulfate Hemihydrate: Experimental and Molecular Dynamics Simulation Studies. *Chem. Eng. J.* **2015**, *278*, 320−327.
(52) Badens, E.; Veesler, S.; Boistelle, R. Crystallization of Gypsum from Hemihydrate in Presence of Additives. *J. Cryst. Growth* **1999**, *198−199*, 704−709 (PART I).
(53) Xue, Z. H.; Dai, S. X.; Hu, B. B.; Du, Z. L. Effect of Langmuir Monolayer of Bovine Serum Albumin Protein on the Morphology of Calcium Carbonate. *Mater. Sci. Eng., C* **2009**, *29*, 1998−2002.
(54) Xue, Z. H.; Hu, B. B.; Jia, X. L.; Wang, H. W.; Du, Z. L. Effect of the Interaction between Bovine Serum Albumin Langmuir Monolayer and Calcite on the Crystallization of $CaCO_3$ Nanoparticles. *Mater. Chem. Phys.* **2009**, *114*, 47−52.
(55) Xue, Z.; Hu, B.; Dai, S.; Jiang, X.; Wu, S.; Du, Z. Crystallization and Self-Assembly of Calcium Carbonate under Albumin Langmuir Monolayers. *Mater. Chem. Phys.* **2011**, *129*, 315−321.
(56) Chen, W.; Wu, Y. N.; Zhang, B.; Wang, Y.; Li, F.; Qi, Z. Retardation Behavior of Hydration of Calcium Sulfate Hemihydrate (Bassanite) Induced by Sodium Trimetaphosphate (STMP). *CrystEngComm* **2018**, *20*, 1662−1668.
(57) Yin, Y.; Jeong, N.; Minjarez, R.; Robbins, C. A.; Carlson, K. H.; Tong, T. Contrasting Behaviors between Gypsum and Silica Scaling in the Presence of Antiscalants during Membrane Distillation. *Environ. Sci. Technol.* **2021**, *55*, 5335−5346.
(58) Massaro, F. R.; Rubbo, M.; Aquilano, D. Theoretical Equilibrium Morphology of Gypsum ($CaSO_4 \cdot 2H_2O$).1.A Syncretic Strategy to Calculate the Morphology of Crystals. *Cryst. Growth Des.* **2010**, *10*, 2870−2878.
(59) Massaro, F. R.; Rubbo, M.; Aquilano, D. Theoretical Equilibrium Morphology of Gypsum ($CaSO_4 \cdot 2H_2O$). 2. The Stepped Faces of the Main [001] Zone. *Cryst. Growth Des.* **2011**, *11*, 1607−1614.

https://doi.org/10.1021/acs.est.1c04143
Environ. Sci. Technol. XXXX, XXX, XXX−XXX